Nanoporous polymer foams derived from high molecular PS-b-P4VP(PDP)(x) for template-directed synthesis approaches

Tillmann, S. D.; Hermida-Merino, D.; Winter, M.; Cekic-Laskovic, I.; Loos, K.

Published in:
RSC Advances

DOI:
10.1039/c6ra06735b

Publication date:
2016

RSC Advances

PAPER

View Article Online
View Journal | View Issue

Cite this: *RSC Adv.*, 2016, **6**, 52998

Nanoporous polymer foams derived from high molecular PS-*b*-P4VP(PDP)$_x$ for template-directed synthesis approaches

S. D. Tillmann,*[a] D. Hermida-Merino,[b] M. Winter,[a] I. Cekic-Laskovic[a] and K. Loos[c]

Received 14th March 2016
Accepted 24th May 2016

DOI: 10.1039/c6ra06735b

www.rsc.org/advances

Due to their ability to self-assemble into a variety of periodic nanostructures, block copolymers already play an important role in designing diverse functional materials. A refined way to rationally tailor the morphology of a block copolymer system is the incorporation of varying amounts of an amphiphile *e.g.* 3-pentadecylphenol (PDP). In order to identify self-assembled structures suitable for the design of various functional materials, different supramolecular complexes of polystyrene-*block*-poly(4-vinylpyridine)(PDP)$_x$ (PS-*b*-P4VP(PDP)$_x$) were prepared and mophologically characterized by small-angle X-ray scattering and scanning electron microscopy techniques. Thereby, the focus was set on the cylindrical-to-lamellar region with a minor P4VP(PDP)$_x$ block. For the first time, the lamellar-in-gyroid morphology was obtained directly by an annealing process. After amphiphile removal, apart from the nanoporous gyroid polymer foam, exceptionally long-range ordered polymer networks with cylindrical pores were obtained. The manifold possible applications of the self-assembled polymer morphologies were exemplarily validated by a template-directed formation of a bicontinuous nickel network *via* electroless plating.

Introduction

Solid materials characterized by their defined structural and functional nature are of great importance in diverse industrial fields. In particular this is evident for processes taking place at the solid–liquid/gaseous interface such as catalysis, electrochemical reactions or absorption processes, where materials with defined morphologies and high surface areas are required. In this regard, block copolymers are a promising class of materials. Thus, in recent years extensive research has been devoted to block copolymers and their potential nanoscale applications.[1–3] Composed of two or more chemically distinct monomer units, block copolymers are able to segregate into nanometer sized phase domains leading to a variety of accessible morphologies. Thereby, the phase behaviour of an individual block copolymer system is mainly dependent on three parameters, namely the relative length of one block f, the Flory–Huggins parameter χ that describes the interaction between the different blocks and, finally, the degree of polymerization N of the polymer system. Polymer morphologies ranging from classical phases like lamellar (LAM) and cylindrical (CYL) structures to more complex phases such as the (double) gyroid morphology (GYR) have been reported.[4–6] In order to obtain a desired morphology, the aforementioned system parameters (f, χ, N) need to be carefully selected. Usually, controlled synthesis is necessary to study the phase behaviour of a certain block copolymer system stepwise. Though, the morphological study of a block copolymer system can be simplified and accelerated using the supramolecular principle. By the addition of either different amphiphiles or varying amounts of amphiphilic compounds, the morphology of the whole amphiphile/block copolymer system can be tailored to a specific purpose.[2,7–9] Furthermore, Yoo *et al.* recently reported on the possibility to tailor the pore size and the porosity of polymeric templates by introducing the surface energy-modifying agent 3-(glycidoxypropyl)trimethoxysilane into one consistent block of an amphiphilic block copolymer system.[10] Supramolecular complexes involving polystyrene-*block*-poly(4-vinylpyridine) (PS-*b*-P4VP) and the low weight molecular amphiphile 3-pentadecylphenol (PDP) *via* formation of hydrogen bonds of the PDP to the P4VP block, have been widely studied.[11–20] In this system, phase separation occurs at two different length scales resulting in structure-within-structure morphologies. First, the diblock copolymer segregates into two blocks (on a scale of 20–100 nm) according to the discussed parameters and second, the non-polar alkyl tails of the PDP microphase separate from P4VP and orientate perpendicular to the domain on a scale of 3–5 nm.[21] The phase diagram of PS-*b*-P4VP(PDP)$_x$ with x being the ratio between PDP molecules and P4VP monomer units

[a]*MEET Battery Research Center, University of Muenster, Corrensstr. 46, 48149 Muenster, Germany. E-mail: Selina.Tillmann@wwu.de*

[b]*BM26/DUBBLE, ESRF-The European Synchrotron, CS40220, 38043 Grenoble Cedex 9, France*

[c]*University of Groningen, Department of Polymer Chemistry & Zernike Institute for Advanced Materials, Nijenborgh 4, NL-9747AG Groningen, The Netherlands*

contains apart from classical morphologies, more complex structures like the hexagonally perforated layers (HPL) or GYR. For the latter, samples in the composition range 0.59 < f(P4VP(PDP)$_x$) < 0.65 were investigated.[16,22] Apart from tuning the long-length scale morphology of the supramolecular complex by varying the PDP amount, this approach offers a further advantage. Nanoporous polymer materials can be generated by immersing the polymer film in ethanol, a selective solvent for PDP, which leads to the formation of a PS core and a P4VP corona.[23] In contrast to block copolymers like polystyrene-*b*-poly(lactic acid) (PS-*b*-PLA), where the removal of the sacrificial block results in a hydrophobic PS surface, in this approach a hydrophilic surface can be exposed. Thus, the well-ordered nanoporous polymer films can be directly processed without further modifications using water-based plating reagents for successful metal deposition into the pores. Recently, Vukovic *et al.* adopted the supramolecular route for the template-directed synthesis of nickel nanofoams.[22] In particular, self-assembled structures with P4VP(PDP)$_x$ displaying the network channels are of great interest due to the manifold template-directed synthesis for nanoscale applications. Therefore, the focus of this study lies on the identification of polymer morphologies in bulk films, which upon removal of the amphiphile give rise to long-range ordered nanoporous matrices suitable for the design of manifold functional materials.

Results and discussion

In particular, three-dimensional polymer nanostructures like the bicontinuous gyroid morphology are of great interest for template-directed synthesis purposes. In case of the supramolecular complex PS-*b*-P4VP(PDP)$_x$ this self-assembled structure has only been described for the P4VP(PDP)$_x$ part being the major component.[16,20] In this study, various supramolecular complexes of PS-*b*-P4VP(PDP)$_x$ with the latter block being the minor part 0.4 < f(P4VP(PDP)) < 0.5, were investigated. As mentioned earlier, adjusting the amount of the amphiphile, the weight fraction of the polymer blocks in the supramolecular complex and, thus, the morphology of the whole system can be changed. Additionally, altering the molecular weight of the parent block copolymer allows a movement along the *y*-axis of the phase diagram. The PDP amount was systematically changed for each block copolymer system and morphological characterized. However, in this paper the focus is set on the supramolecular complexes with the most interesting obtained morphologies (Table 1).

Table 1 Supramolecular complexes PS-*b*-P4VP(PDP)$_x$ discussed in this study

Polymer sample	x(PDP)	f(P4VP(PDP))	Morphology at RT
PP-40.5-16.5	0.5	0.49	Lam-in-LAM
PP-93-35	0.4	0.45	Lam-in-CYL
PP-190-64	0.5	0.46	Lam-in-GYR
PP-330-125	0.5	0.42	Lam-in-CYL

Polymer films were prepared by solvent-casting of the block copolymer together with the specific amounts of PDP in *N*,*N*-dimethylformamide. After solvent and thermal annealing, the morphology of the samples was investigated by the following methods. First, small-angle X-ray scattering (SAXS) experiments were performed in order to identify promising supramolecular structures (Fig. 1). For the first complex PP-40.5-16.5, four diffraction peaks positioned in the q ratio 1 : 2 : 3 : 4 were observed, indicating the presence of the lam-in-LAM morphology (Fig. 1a). The lamellar structure of 40 nm follows from the first order-reflection peak at $q^* = 0.157$ nm^{-1}. In addition, the peak positioned at $q = 1.62$ nm^{-1} can be attributed to lamellar structures with the lamellar period of 3.9 nm^{-1}, which are formed in the comb-like block P4VP(PDP)$_{0.6}$ due to microphase separation between the nonpolar PDP alkyl trails and the polar backbone.[24] Indeed, the distinct peak could only be observed in the case of PP-40.5-16.5 due to measuring device limitations. However, based on literature structure-within-structure morphologies, namely lam-within-structures, can be assumed for the following polymer samples.[23] By increasing the molar fraction of P4VP(PDP) to 0.45 in case of the polymer sample PP-93-35 the phase diagram in the region between CYL and LAM in the high (N > 1000) molecular weight region can be further characterized. The SAXS curve (Fig. 1b) contains four dominant peaks at q^*, $\sqrt{3}q^*$, $\sqrt{4}q^*$ and $\sqrt{7}q^*$ being characteristic for the CYL morphology. With the first-order reflection at $q^* = 0.077$ nm^{-1}, the size of the unit cell is 82 nm. On the other hand in the SAXS pattern of the polymer sample PP-190-64 with a molar fraction of 0.46 of the comb-like block, characteristic Bragg reflections for the double gyroid morphology are revealed at $\sqrt{2}q^*$, $\sqrt{6}q^*$, $\sqrt{8}q^*$, $\sqrt{10}q^*$, $\sqrt{14}q^*$, $\sqrt{24}q^*$, $\sqrt{40}q^*$ (Fig. 1c). These peaks were indexed as reflections from (110), (221), (220), (310), (321), (422) and (620) planes. The first intensity maximum is located at $q^* = 0.054$ nm^{-1} which corresponds to the d_{110} spacing equal to 116 nm and the lattice parameter a being 164 nm ($a = \sqrt{2}d_{110}$). Hence, the bicontinuous gyroid morphology could be observed in the supramolecular complex PS-*b*-P4VP(PDP)$_x$ with the latter block being the minority directly after annealing. In the past, double gyroid morphologies were already obtained for high-molecular weight polymers for instance by the groups of Matsushita and Thomas for polystyrene-*b*-polyisoprene (PS-*b*-PI) block copolymers.[25,26] Theoretical calculations by Cochran *et al.* supported the findings stating that the gyroid morphology is present as an equilibrium microdomain structure in the weak to the strong segregation range.[6,27] Presumably, the presence of the PDP reduces the interfacial tension between the PS phase and the P4VP(PDP)$_x$ due to the enrichment of the interface with amphiphiles (PDP) rendering the system to behave as in the intermediate segregation regime, so that even in the high-molecular weight block copolymer sample PP-190-64 the more complex phase occurs.[28] Finally, for the highest molecular weight polymer sample PP-330-125, CYL morphology can be identified from the typical Bragg reflections (Fig. 1d). The first-order reflection at $q^* = 0.054$ (hence, the distance between the cylinders is 116 nm) is followed by further intensity maxima at $\sqrt{3}q^*$, $\sqrt{4}q^*$, $\sqrt{7}q^*$ and $\sqrt{12}q^*$.

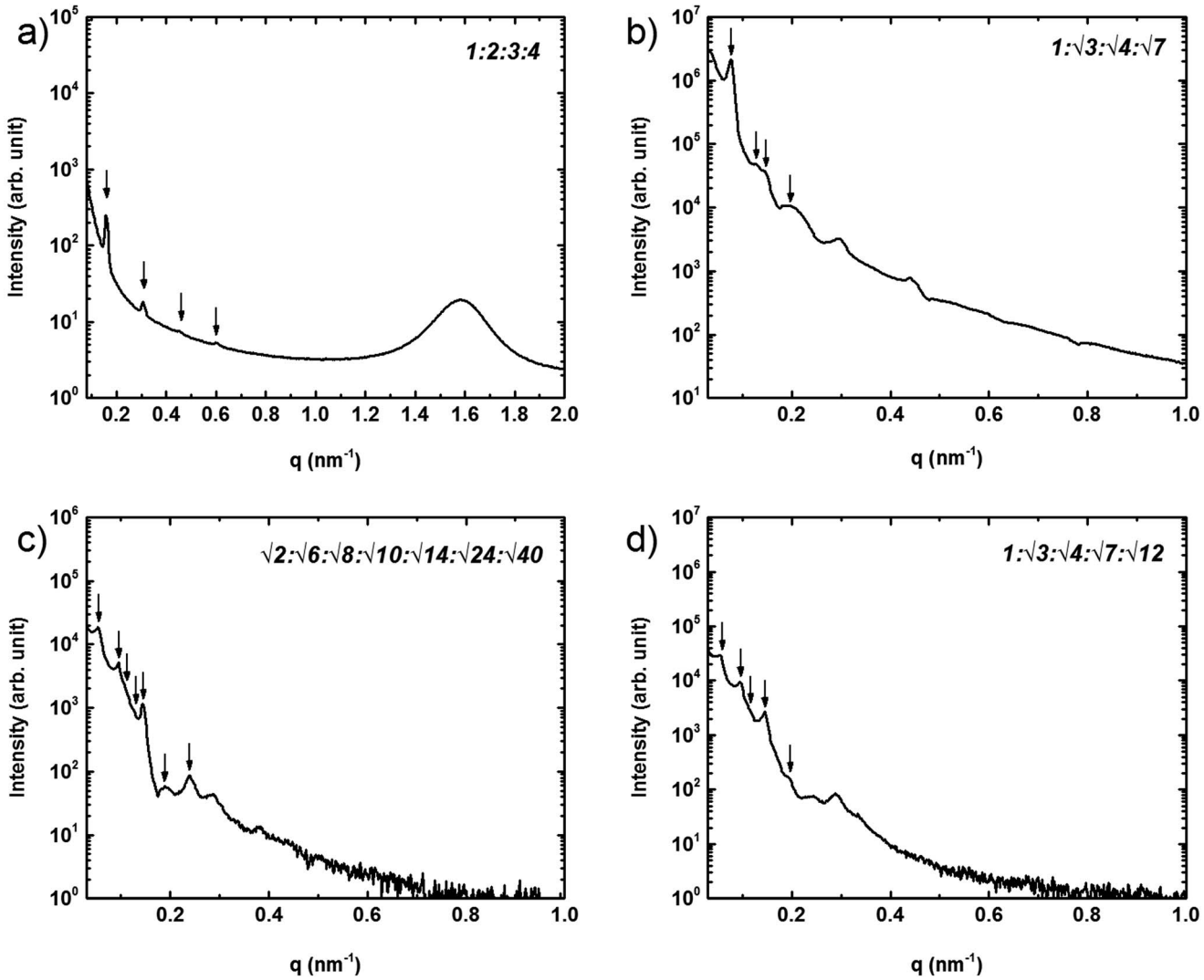

Fig. 1 SAXS intensity patterns of various bulk polymer films: (a) characteristic lamellar reflections observed for the polymer sample PP-40.5-16.5 with $x = 0.5$ and f(P4VP(PDP)) = 0.49, (b) polymer sample PP-93-35 with $x = 0.4$ and f(P4VP(PDP)) = 0.45 indicating the cylindrical morphology, (c) polymer sample PP-190-64 with $x = 0.5$ and f(P4VP(PDP)) = 0.46 showing characteristic gyroid intensity maxima and, finally, (d) cylindrical morphology found in polymer sample PP-330-125, $x = 0.5$, f(P4VP(PDP)) = 0.42.

Porous polymer foams were generated by washing the films with ethanol to selectively remove the amphiphilic additive. Fig. 2 displays scanning electron microscopy (SEM) images of the polymer samples PP-40.5-16.5, PP-93-35 and PP-190-64. With respect to the specific morphology characteristics and size, different magnifications were utilized. As visible in the micrograph of the lamellar polymer sample PP-40.5-16.5 (Fig. 2a) the lamellas collapsed onto each other, so that no free-standing matrix can be generated. Even if the polymer sample is directly processed after amphiphile removal in a wet state, *e.g.* by electroless plating, the matrix collapse is inevitable.[29] Therefore, the lamellar morphology of this polymer cannot be considered for template-directed synthesis approaches. Exemplarily for the formation of a cylindrical nanoporous film, SEM images of the sample PP-93-35 are depicted in Fig. 2b and c. During annealing, the P4VP(PDP) microphase separates from the PS domain and P4VP(PDP) cylinders in a matrix of PS are formed. Removal of the PDP gives rise to a cylindrical perforated matrix. Thereby, a parallel alignment of the cylinders to the substrate is observed (Fig. 2b). Taking a closer look perpendicular to the top-down direction, terraces within the structure can be identified (Fig. 2c). In accordance with previous phase behaviour studies, although performed for thin films,[17,18] this alignment can be attributed to the strong preference of the amphiphile PDP to the air. In particular, the long-range stability of this porous polymer matrix is remarkable, which makes it suitable as template for the preparation of nanowires or nanotubes. Nevertheless, for applications where a continuous, three-dimensional pore system is required, the gyroid morphology is of great interest. As already indicated in the SAXS pattern of sample PP-190-64, the presence of this structure is ascertained (Fig. 2d). The typical double-wave pattern representing the projection through the (211) gyroid plane are observed. Finally, the polymer film

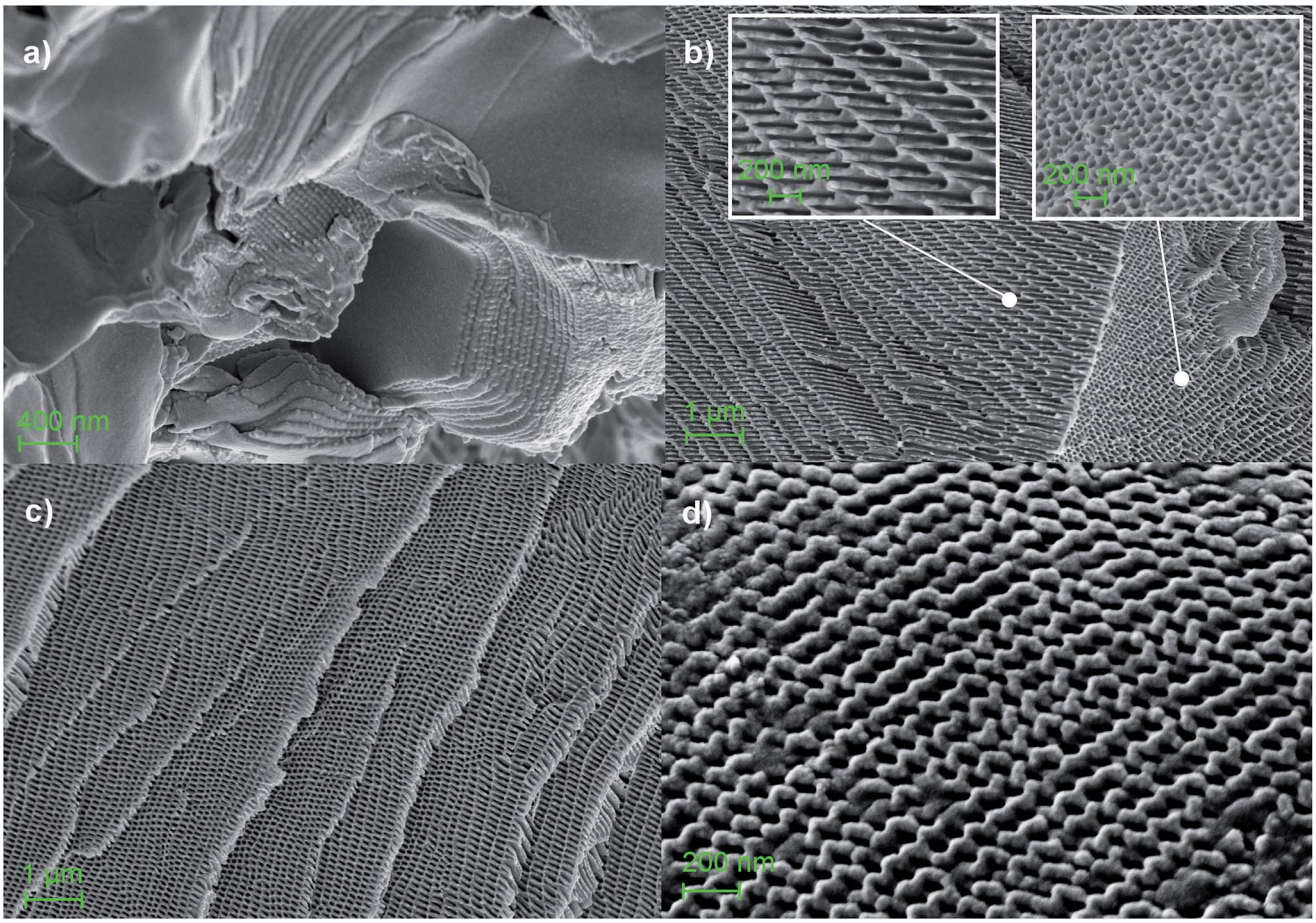

Fig. 2 SEM micrographs of the polymer films obtained after removal of the amphiphile with (a) collapsed lamellas visible for the polymer sample PP-40.5-16.5 (25k-fould magnification). The following two images (b) and (c) show parallel alignment of the cylindrical pores (top-down view) and the typical terrace structure (coaxial view) in the polymer sample PP-93-35, respectively (both 10k-fould magnification). Additionally, for (b) insets of the pores are included (25k-fould magnification). In (d) the typical double-wave pattern verifying the presence of the double gyroid morphology for polymer sample PP-190-64 is depicted (50k-fold magnification).

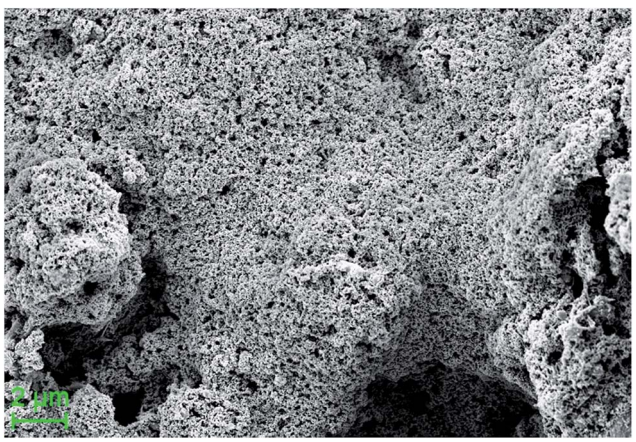

Fig. 3 SEM micrograph of the bicontinuous nanoporous nickel network obtained by template-directed electroless plating of the gyroid polymer foam (PP-190-64) and followed by thermal degradation of the organic matrix.

Table 2 Characteristics of investigated polymer samples PS-*b*-P4VP

Polymer sample	M_n (PS) (kg mol^{-1})	M_n (P4VP) (kg mol^{-1})	M_n (PS)/M_n (P4VP)	PDI[a]
PP-40.5-16.5	40.5	16.5	2.45	1.18
PP-93-35	93	35	2.66	1.15
PP-190-64	190	64	2.97	1.14
PP-330-125	330	125	2.64	1.18

[a] Data sheet (Polymer Source Inc.).

representing the double gyroid morphology is used as a template for electroless nickel plating. As evidenced in Fig. 3, a freestanding nickel replica is obtained upon thermal degradation of the organic template.

Conclusions

The phase behaviour of higher-molecular weight supramolecular complexes of PS-*b*-P4VP(PDP)$_x$ with P4VP(PDP)$_x$ being the

minor component was thoroughly studied by means of SAXS and SEM techniques. Apart from the notably long-range ordered lam-in-CYL morphology, which is suitable for the template-directed synthesis of defined nanotubes, the lam-in-GYR morphology could be obtained for the first time directly after annealing. After removal of the amphiphile the nanoporous polymer structure can be further processed *via* electroless plating. Thus, the bicontinuous nickel network derived from the supramolecular complex PS-*b*-P4VP(PDP)$_x$ is now accessible for various nanoscale applications. Bicontinuous gyroid metal structures typically feature a high surface area. Combined with their highly ordered structure, which leads to excellent mechanical properties of the overall system, they are suitable for the application in catalysis and for the preparation of nanostructured electrodes for advanced electrochemical energy storage applications.

Experimental

Materials

Diblock polymers of polystyrene-*block*-poly(4-vinylpyridine) (PS-*b*-P4VP) were received from Polymer Source Inc. and their specific properties are summed up in Table 2. Unless otherwise stated, all chemicals used during this study were purchased from Sigma-Aldrich. 3-Pentadecylphenol (PDP, 90%) was recrystallized triply from petroleum ether and dried under reduced pressure prior to use. Other agents were used as received.

Preparation of polymer foams

Polymer films of the supramolecular complexes were prepared by dissolving the appropriate amount of PS-*b*-P4VP block copolymer together with 3-PDP in *N*,*N*-dimethylformamide (DMF, 99.8%). To ensure homogeneous complex formation the concentration of the solution was adjusted to 1.8 wt%. After stirring for three hours the solution is poured into a petri dish, covered with filter paper and placed into a saturated DMF atmosphere. Thereafter, the solvent was allowed to slowly evaporate at 45 °C over several days and the films were dried at 30 °C in an oven overnight under vacuum. Thermal annealing of the polymer films was performed at 120 °C for three days in a nitrogen atmosphere with 1 bar overpressure. Finally, the samples were cooled down to room temperature over five hours. Polymer foams were generated by stirring the as prepared films for three days in ethanol.

Formation of nickel foam

The polymer-nickel nanohybrid was prepared by electroless plating. The procedure involved a sensitization step of the polymer pores, an activation step for the generation of the catalyst which, finally, promoted the nickel plating onto the polymer scaffold. All plating solutions were freshly prepared prior to the experiments. For sensitization of the pores' surface the polymer foam was stirred in a Sn^{2+}-solution (0.09 mol L^{-1} tin(II) chloride (98%), 0.48 mol L^{-1} hydrochloric acid (HCl, 37%) in water : ethanol (99.8%) 1 : 1 (w/w) for one hour and was rinsed gently with a water–ethanol solution. Afterwards, the sample was immersed in a Pd^{2+}-solution (1.24 mmol L^{-1} palladium(II) chloride (60% Pd basis), 0.48 mol L^{-1} HCl in water : ethanol 1 : 1 (w/w) for another hour. In order to remove redundant Pd^{2+} from the surface, the polymer foam was stirred in a water–ethanol solution for several minutes. The final plating of the polymer samples was performed in a constantly stirred water-based nickel bath comprising 0.26 mol L^{-1} nickel(II) sulfate hexahydrate (99%), 0.08 mol L^{-1} citric acid trisodium salt (≥98%), 0.11 mol L^{-1} lactic acid solution (≥85%) and borane dimethyl amine complex (97%) during one hour. The pH of the plating solution was adjusted to 7.0 using ammonium hydroxide (28–30% NH_3 basis). After drying of the polymer-nickel nanohybrid it was placed in a tube furnace (robatherm). Thermal degradation of the polymer foams was performed at 350 °C for 6 hours in an argon atmosphere.

Characterization

Scanning electron microscopy (SEM) was used to investigate the morphology of the different polymer and nickel foams. The samples were analysed with the Auriga CrossBeam workstation from Zeiss at an acceleration voltage of 3 kV and a working distance of 2.0 mm using the InLens detector. Prior to SEM-imaging the polymer foams were sputter-coated with gold (99.99%, ChemPUR) for 30 s at 5 mA (Quorum Technologies Q150T).

Small-angle X-ray scattering (SAXS) experiments of the polymer films were performed at the Dutch-Belgian beamline (DUBBLE) station BM26B of the European Synchrotron Radiation Facility (ESRF) in Grenoble (France). The sample-to-detector distance was *ca.* 7.3 m and the wavelength $\lambda = 1.033$ Å. The SAXS patterns were recorded using a Dectris-Pilatus 1 M detector with a resolution of 981 × 1048 pixels and a pixel size of 172 × 172 μm. Standard corrections for the sample absorption and background subtractions were performed. In order to correct primary beam fluctuations the raw data were normalized with respect to the incident beam intensity. For calibrating the wave detector scale of the scattering curve the scattering patterns from rat tail were used. All shown SAXS patterns were recorded at room temperature. The scattering vector q is defined as $q = 4\pi/\lambda \times \sin(\theta)$ with 2θ being the scattering angle.[17,30–32]

Acknowledgements

Beam time on the Dutch-Belgian Beamline (DUBBLE) of the European Synchrotron Radiation Facility (ESRF, Grenoble, France) has kindly been made available by The Netherlands Organisation for Scientific Research (NWO). Additionally, Vincent Voet and Anton Hofman are gratefully acknowledged for guidance and beneficial discussions regarding SAXS experiments.

References

1 D. R. Rolison, J. W. Long, J. C. Lytle, A. E. Fischer, C. P. Rhodes, T. M. McEvoy, M. E. Bourg and A. M. Lubers, *Chem. Soc. Rev.*, 2009, **38**, 226–252.

2 O. Ikkala and G. ten Brinke, *Chem. Commun.*, 2004, 2131–2137.
3 J. Kao, K. Thorkelsson, P. Bai, B. J. Rancatore and T. Xu, *Chem. Soc. Rev.*, 2013, **42**, 2654–2678.
4 F. S. Bates, *Science*, 1991, **251**, 898–905.
5 J. N. L. Albert and T. H. Epps Iii, *Mater. Today*, 2010, **13**, 24–33.
6 E. W. Cochran, C. J. Garcia-Cervera and G. H. Fredrickson, *Macromolecules*, 2006, **39**, 2449–2451.
7 J.-M. Lehn, in *Supramolecular Chemistry*, Wiley-VCH Verlag GmbH & Co. KGaA, 2006, pp. 81–87.
8 A. H. Hofman, M. Reza, J. Ruokolainen, G. ten Brinke and K. Loos, *Macromolecules*, 2014, **47**, 5913–5925.
9 A. H. Hofman, Y. Chen, G. ten Brinke and K. Loos, *Macromolecules*, 2015, **48**, 1554–1562.
10 S. Yoo, J.-H. Kim, M. Shin, H. Park, J.-H. Kim, S.-Y. Lee and S. Park, *Sci. Adv.*, 2015, **1**, e1500101.
11 Y. Sageshima, S. Arai, A. Noro and Y. Matsushita, *Langmuir*, 2012, **28**, 17524–17529.
12 W. van Zoelen, S. Bondzic, T. F. Landaluce, J. Brondijk, K. Loos, A.-J. Schouten, P. Rudolf and G. t. Brinke, *Polymer*, 2009, **50**, 3617–3625.
13 I. I. Perepichka, Q. Lu, A. Badia and C. G. Bazuin, *Langmuir*, 2013, **29**, 4502–4519.
14 G. ten Brinke, K. Loos, I. Vukovic and G. G. du Sart, *J. Phys.: Condens. Matter*, 2011, **23**, 284110–284116.
15 T. Ruotsalainen, J. Turku, P. Hiekkataipale, U. Vainio, R. Serimaa, G. ten Brinke, A. Harlin, J. Ruokolainen and O. Ikkala, *Soft Matter*, 2007, **3**, 978–985.
16 S. Valkama, T. Ruotsalainen, A. Nykänen, A. Laiho, H. Kosonen, G. ten Brinke, O. Ikkala and J. Ruokolainen, *Macromolecules*, 2006, **39**, 9327–9336.
17 W. van Zoelen, T. Asumaa, J. Ruokolainen, O. Ikkala and G. ten Brinke, *Macromolecules*, 2008, **41**, 3199–3208.
18 W. van Zoelen, E. Polushkin and G. ten Brinke, *Macromolecules*, 2008, **41**, 8807–8814.
19 I. Vukovic, G. ten Brinke and K. Loos, *Macromolecules*, 2012, **45**, 9409–9418.
20 I. Vukovic, T. P. Voortman, D. H. Merino, G. Portale, P. Hiekkataipale, J. Ruokolainen, G. ten Brinke and K. Loos, *Macromolecules*, 2012, **45**, 3503–3512.
21 G. Gobius du Sart, I. Vukovic, G. Alberda van Ekenstein, E. Polushkin, K. Loos and G. ten Brinke, *Macromolecules*, 2010, **43**, 2970–2980.
22 I. Vukovic, S. Punzhin, Z. Vukovic, P. Onck, J. T. M. De Hosson, G. ten Brinke and K. Loos, *ACS Nano*, 2011, **5**, 6339–6348.
23 T. Ruotsalainen, J. Turku, P. Heikkilä, J. Ruokolainen, A. Nykänen, T. Laitinen, M. Torkkeli, R. Serimaa, G. ten Brinke, A. Harlin and O. Ikkala, *Adv. Mater.*, 2005, **17**, 1048–1052.
24 J. Ruokolainen, M. Torkkeli, R. Serimaa, B. E. Komanschek, O. Ikkala and G. ten Brinke, *Phys. Rev. E: Stat., Nonlinear, Soft Matter Phys.*, 1996, **54**, 6646–6649.
25 Y. Matsushita, J. Suzuki and M. Seki, *Phys. B*, 1998, **248**, 238–242.
26 A. M. Urbas, M. Maldovan, P. DeRege and E. L. Thomas, *Adv. Mater.*, 2002, **14**, 1850–1853.
27 N. Politakos, E. Ntoukas, A. Avgeropoulos, V. Krikorian, B. D. Pate, E. L. Thomas and R. M. Hill, *J. Polym. Sci., Part B: Polym. Phys.*, 2009, **47**, 2419–2427.
28 E. Polushkin, G. O. R. Alberda van Ekenstein, M. Knaapila, J. Ruokolainen, M. Torkkeli, R. Serimaa, W. Bras, I. Dolbnya, O. Ikkala and G. ten Brinke, *Macromolecules*, 2001, **34**, 4917–4922.
29 V. S. D. Voet, D. Hermida-Merino, G. ten Brinke and K. Loos, *RSC Adv.*, 2013, **3**, 7938–7946.
30 W. Bras, I. P. Dolbnya, D. Detollenaere, R. van Tol, M. Malfois, G. N. Greaves, A. J. Ryan and E. Heeley, *J. Appl. Crystallogr.*, 2003, **36**, 791–794.
31 G. Portale, D. Cavallo, G. C. Alfonso, D. Hermida-Merino, M. van Drongelen, L. Balzano, G. W. M. Peters, J. G. P. Goossens and W. Bras, *J. Appl. Crystallogr.*, 2013, **46**, 1681–1689.
32 M. Borsboom, W. Bras, I. Cerjak, D. Detollenaere, D. Glastra van Loon, P. Goedtkindt, M. Konijnenburg, P. Lassing, Y. K. Levine, B. Munneke, M. Oversluizen, R. van Tol and E. Vlieg, *J. Synchrotron Radiat.*, 1998, **5**, 518–520.